Solid State Nuclear Magnetic Resonance, 2 (1993) 165–180
Elsevier Science Publishers B.V., Amsterdam

Determination of spin-5/2 quadrupolar coupling with two-pulse sequences

Pascal P. Man

Laboratoire de Chimie des Surfaces, CNRS URA 1428, Université Pierre et Marie Curie, 4 Place Jussieu, Tour 55, 75252 Paris Cedex 05, France

(Received 1 April 1993; accepted 4 May 1993)

Abstract

The density matrix of a spin-5/2 system excited by two in-phase pulses separated by a delay τ_2 is calculated from the equilibrium state to the end of the second pulse. The interaction involved throughout the computation is the first-order quadrupolar interaction. Consequently, the results are valid for any ratio of the quadrupolar coupling to the amplitude of the radio-frequency pulse. It is shown that single- and multi-quantum coherences developed during the first pulse are detected at the end of the second pulse through single-quantum coherences. Other two-pulse sequences with various phase cyclings as well as the rotary echo sequence are also discussed and illustrated with the nuclei ^{27}Al in a single crystal of corundum Al_2O_3.

Keywords: ^{27}Al NMR; quadrupolar interaction; spin-5/2; two-pulse excitation

Introduction

There is a great deal of interest in spin-5/2 systems, for instance, ^{27}Al [1,2], ^{17}O [3] or ^{95}Mo [4] in inorganic chemistry [5] have led to both experimental and theoretical developments in solid-state NMR. These nuclei are sensitive to the electric field gradient (EFG) of their surroundings. Therefore, they should provide valuable information about their local symmetry. The major technique applied for determining the physical parameters (quadrupolar coupling constant e^2qQ/h, asymmetry parameter η, and second-order quadrupolar shift δ_{QS}) is the popular magic-angle spinning of the sample at very high speed [6,7]. Other techniques like two-dimensional Fourier transform methods [8–10], or cross-polarization [11] are also investigated. Surprisingly, the spin-echo sequences [12–16] in common use for recovering broad lines lost in the dead time of the receiver are not well studied. Lost of ^{27}Al signals happens very often in zeolite characterization [17,18] with a single radio-frequency pulse excitation.

The present paper, which extends our previous study [19] on the time domain response of a spin-5/2 system excited by a single pulse, represents an important step toward the investigation of the Solomon echoes [15,16]. A second in-phase pulse is introduced after a delay τ_2 from the first pulse. The analytical expression of the line intensity of the central transition and those of the two satellite transitions are obtained using software called Mathematica. As a result, the spin dynamics at the end of this second pulse is discussed. Furthermore, other two-pulse sequences with various phase cyclings and the rotary echo sequence are also analyzed and illustrated with the nuclei ^{27}Al in a single crystal of corundum Al_2O_3.

Theory

The Hamiltonians throughout the paper are defined in angular frequency units. Neglecting relaxation phenomena and second-order quadrupolar effects, the dynamics of a spin $I = 5/2$ system excited by two $-x$ pulses (Fig. 1) is described, at the end of the second pulse, by the density matrix $\rho(t_1, \tau_2, t_3)$ expressed in the rotating frame associated with the central transition:

$$\rho(t_1, \tau_2, t_3) = \exp\left(-i\mathcal{H}^{(-x)}t_3\right) \exp\left(-i\mathcal{H}_Q^{(1)}\tau_2\right) \exp\left(-i\mathcal{H}^{(-x)}t_1\right)\rho(0)$$
$$\times \exp\left(i\mathcal{H}^{(-x)}t_1\right) \exp\left(i\mathcal{H}_Q^{(1)}\tau_2\right) \exp\left(i\mathcal{H}^{(-x)}t_3\right) \quad (1)$$

where

$$\rho(0) = I_z \quad (2a)$$

$$\mathcal{H}_{rf} = \omega_{rf} I_x \quad (2b)$$

$$\omega_Q = \frac{3e^2qQ}{8I(2I-1)\hbar}\left[3\cos^2\beta - 1 + \eta \sin^2\beta \cos 2\alpha\right] \quad (2c)$$

$$\mathcal{H}_Q^{(1)} = \tfrac{1}{3}\omega_Q\left[3I_z^2 - I(I+1)\right] \quad (2d)$$

$$\mathcal{H}^{(-x)} = \mathcal{H}_{rf} + \mathcal{H}_Q^{(1)} \quad (2e)$$

$\mathcal{H}_Q^{(1)}$ is the first-order quadrupolar interaction. The Euler angles α and β describe the orientation of the strong static magnetic field in the principal axis system of the EFG tensor. In particular, ω_{rf} and ω_Q are the amplitude of the pulse and the quadrupolar coupling defined experimentally by half of the frequency separating two consecutive lines in a spectrum of a single crystal (a definition among others), respectively. As relaxation phenomena are not considered, the value of τ_2 must be much smaller than the duration of the free induction decay (fid). Eqn. (1) can be expressed with Ω and T_1, the matrices of eigenvalues and eigenvectors of $\mathcal{H}^{(-x)}$ [19], respectively,

$$\rho(t_1, \tau_2, t_3) = T_1 \exp(-i\Omega t_3)T_1^{-1} \exp\left(-i\mathcal{H}_Q^{(1)}\tau_2\right)\rho(t_1) \exp\left(i\mathcal{H}_Q^{(1)}\tau_2\right)T_1 \exp(i\Omega t_3)T_1^{-1} \quad (3)$$

The density matrix $\rho(t_1)$ and its associated parameters describing the spin system at the end of the first $-x$ pulse were obtained previously [19]. The three components ($X_{m\pm}$, $Y_{m\pm}$, $Z_{m\pm}$) of the six normalized

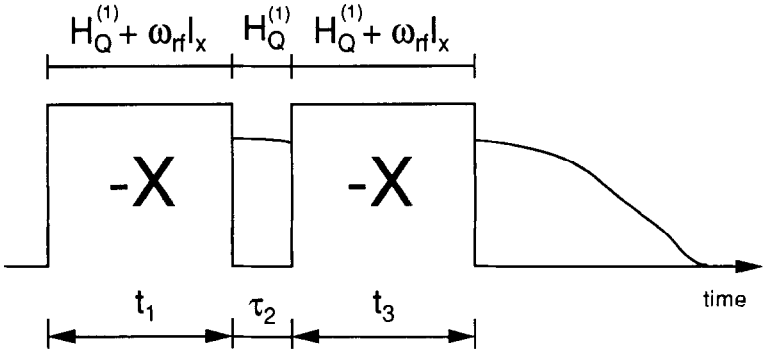

Fig. 1. Hamiltonians and time domain parameters associated with the sequence {$-x$}–τ_2–{$-x$}–[acquisition(y)]–recycle delay.

TABLE 1

Parameters defined for a $-x$ pulse ($m = 1, 2, 3$) from ref. 19

$$\omega_{1+} = -\frac{\omega_{rf}}{2} + 2\sqrt{\frac{s_+}{3}}\cos\frac{\phi_+}{3} \qquad \omega_{1-} = \frac{\omega_{rf}}{2} + 2\sqrt{\frac{s_-}{3}}\cos\frac{\phi_-}{3}$$

$$\omega_{2+} = -\frac{\omega_{rf}}{2} - 2\sqrt{\frac{s_+}{3}}\cos\left(\frac{\pi}{3} - \frac{\phi_+}{3}\right) \qquad \omega_{2} = \frac{\omega_{rf}}{2} - 2\sqrt{\frac{s_-}{3}}\cos\left(\frac{\pi}{3} - \frac{\phi_-}{3}\right)$$

$$\omega_{3+} = -\frac{\omega_{rf}}{2} - 2\sqrt{\frac{s_+}{3}}\cos\left(\frac{\pi}{3} + \frac{\phi_+}{3}\right) \qquad \omega_{3-} = \frac{\omega_{rf}}{2} - 2\sqrt{\frac{s_-}{3}}\cos\left(\frac{\pi}{3} + \frac{\phi_-}{3}\right)$$

$$s_\pm = \tfrac{84}{9}\omega_Q^2 \pm 4\omega_Q\omega_{rf} + 4\omega_{rf}^2 \qquad q_\pm = \frac{\omega_Q}{27}\left(160\omega_Q^2 \pm 36\omega_Q\omega_{rf} - 144\omega_{rf}^2\right)$$

$$\cos\phi_+ = \frac{3q_-}{2s_+}\sqrt{\frac{3}{s_+}} \qquad \cos\phi_- = \frac{3q_+}{2s_-}\sqrt{\frac{3}{s_-}}$$

$$X_{m\pm} = \frac{x_{m\pm}}{Q_{m\pm}} \qquad Y_{m\pm} = \frac{y_{m\pm}}{Q_{m\pm}} \qquad Z_{m\pm} = \frac{z_{m\pm}}{Q_{m\pm}}$$

$$x_{m+} = -\frac{\sqrt{5}\,\omega_{rf}}{2a_{m+}} \qquad x_{m-} = \frac{\sqrt{2}\,\omega_{rf}}{b_{m-}}$$

$$y_{m+} = 1 \qquad y_{m-} = 1$$

$$z_{m+} = \frac{\sqrt{2}\,\omega_{rf}}{b_{m+}} \qquad z_{m-} = -\frac{\sqrt{5}\,\omega_{rf}}{2a_{m-}}$$

$$a_{m\pm} = \tfrac{10}{3}\omega_Q - \omega_{m\pm} \qquad b_{m\pm} = \tfrac{8}{3}\omega_Q \pm \tfrac{3}{2}\omega_{rf} + \omega_{m\pm}$$

$$Q_{m\pm} = \sqrt{1 + \frac{5\omega_{rf}^2}{4a_{m\pm}^2} + \frac{2\omega_{rf}^2}{b_{m\pm}^2}}$$

eigenvectors associated with the six eigenvalues $\omega_{m\pm}$ are gathered in Table 1. On the other hand, the components of $\rho(t_1)$ written as 'line intensities',

$$\langle I_k^{m,n} \rangle = \mathrm{Tr}\left[\rho(t_1) I_k^{m,n}\right] \tag{4}$$

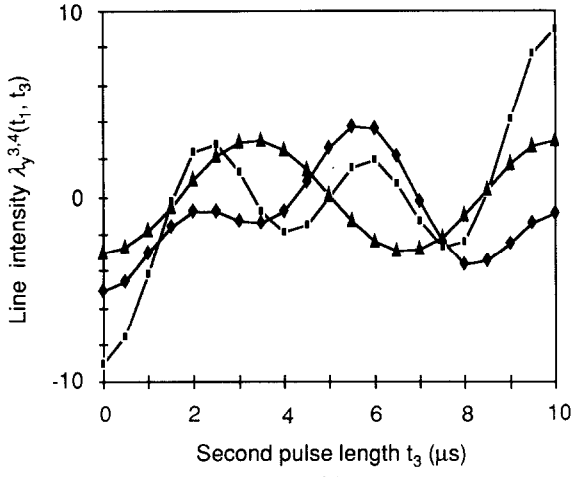

Fig. 2. Theoretical line intensity $\lambda_y^{3,4}(t_1, t_3)$, eqn. (10), *versus* t_3 for three couples of $(\omega_Q/2\pi, t_1)$ values: ■ (0 kHz, 5 μs), ♦ (50 kHz, 3 μs), and ▲ (1 MHz, 1.66 μs); $\omega_{rf}/2\pi = 50$ kHz.

TABLE 2

The density matrix $\rho(t_1)$ and its components: for clarity, the symbol $\frac{1}{4}\sum_{m=1}^{3}\sum_{j=1}^{3}K_{mj}$ in front of each term has been omitted, *e.g.*, $\langle I_x^{1,2}\rangle + i\langle I_y^{1,2}\rangle = \frac{1}{4}\sum_{m=1}^{3}\sum_{j=1}^{3}K_{mj}[(X_{m+}Y_{j-} + Y_{m+}Z_{j-})\cos\omega_{mj}t_1 + i(X_{m+}Y_{j-} - Y_{m+}Z_{j-})\sin\omega_{mj}t_1]$ is written as below with $K_{mj} = 5X_{m+}Z_{j-} + 3Y_{m+}Y_{j-} + Z_{m+}X_{j-}$

$$\rho(t_1) = \begin{bmatrix} \langle I_z^{1,6}\rangle & \langle I_x^{1,2}\rangle - i\langle I_y^{1,2}\rangle & \langle I_x^{1,3}\rangle - i\langle I_y^{1,3}\rangle & \langle I_x^{1,4}\rangle - i\langle I_y^{1,4}\rangle & \langle I_x^{1,5}\rangle - i\langle I_y^{1,5}\rangle & -i\langle I_y^{1,6}\rangle \\ \langle I_x^{1,2}\rangle + i\langle I_y^{1,2}\rangle & \langle I_z^{2,5}\rangle & \langle I_x^{2,3}\rangle - i\langle I_y^{2,3}\rangle & \langle I_x^{2,4}\rangle - i\langle I_y^{2,4}\rangle & -i\langle I_y^{2,5}\rangle & -\langle I_x^{1,5}\rangle - i\langle I_y^{1,5}\rangle \\ \langle I_x^{1,3}\rangle + i\langle I_y^{1,3}\rangle & \langle I_x^{2,3}\rangle + i\langle I_y^{2,3}\rangle & \langle I_z^{3,4}\rangle & -i\langle I_y^{3,4}\rangle & -\langle I_x^{2,4}\rangle - i\langle I_y^{2,4}\rangle & -\langle I_x^{1,4}\rangle - i\langle I_y^{1,4}\rangle \\ \langle I_x^{1,4}\rangle + i\langle I_y^{1,4}\rangle & \langle I_x^{2,4}\rangle + i\langle I_y^{2,4}\rangle & i\langle I_y^{3,4}\rangle & -\langle I_z^{3,4}\rangle & -\langle I_x^{2,3}\rangle - i\langle I_y^{2,3}\rangle & -\langle I_x^{1,3}\rangle - i\langle I_y^{1,3}\rangle \\ \langle I_x^{1,5}\rangle + i\langle I_y^{1,5}\rangle & i\langle I_y^{2,5}\rangle & -\langle I_x^{2,4}\rangle + i\langle I_y^{2,4}\rangle & -\langle I_x^{2,3}\rangle + i\langle I_y^{2,3}\rangle & -\langle I_z^{2,5}\rangle & -\langle I_x^{1,2}\rangle - i\langle I_y^{1,2}\rangle \\ i\langle I_y^{1,6}\rangle & -\langle I_x^{1,5}\rangle + i\langle I_y^{1,5}\rangle & -\langle I_x^{1,4}\rangle + i\langle I_y^{1,4}\rangle & -\langle I_x^{1,3}\rangle + i\langle I_y^{1,3}\rangle & -\langle I_x^{1,2}\rangle + i\langle I_y^{1,2}\rangle & -\langle I_z^{1,6}\rangle \end{bmatrix}$$

$$\langle I_z^{1,6}\rangle = 2X_{m+}Z_{j-}\cos\omega_{mj}t_1 \qquad \langle I_x^{1,2}\rangle + i\langle I_y^{1,2}\rangle = (X_{m+}Y_{j-} + Y_{m+}Z_{j-})\cos\omega_{mj}t_1 + i(X_{m+}Y_{j-} - Y_{m+}Z_{j-})\sin\omega_{mj}t_1$$

$$\langle I_z^{2,5}\rangle = 2Y_{m+}Y_{j-}\cos\omega_{mj}t_1 \qquad \langle I_x^{1,3}\rangle + i\langle I_y^{1,3}\rangle = (X_{m+}X_{j-} + Z_{m+}Z_{j-})\cos\omega_{mj}t_1 + i(X_{m+}X_{j-} - Z_{m+}Z_{j-})\sin\omega_{mj}t_1$$

$$\langle I_z^{3,4}\rangle = 2Z_{m+}X_{j-}\cos\omega_{mj}t_1 \qquad \langle I_x^{1,4}\rangle + i\langle I_y^{1,4}\rangle = (X_{m+}X_{j-} - Z_{m+}Z_{j-})\cos\omega_{mj}t_1 + i(X_{m+}X_{j-} + Z_{m+}Z_{j-})\sin\omega_{mj}t_1$$

$$\langle I_y^{1,6}\rangle = 2X_{m+}Z_{j-}\sin\omega_{mj}t_1 \qquad \langle I_x^{1,5}\rangle + i\langle I_y^{1,5}\rangle = (X_{m+}Y_{j-} - Y_{m+}Z_{j-})\cos\omega_{mj}t_1 + i(X_{m+}Y_{j-} + Y_{m+}Z_{j-})\sin\omega_{mj}t_1$$

$$\langle I_y^{2,5}\rangle = 2Y_{m+}Y_{j-}\sin\omega_{mj}t_1 \qquad \langle I_x^{2,3}\rangle + i\langle I_y^{2,3}\rangle = (Y_{m+}X_{j-} + Z_{m+}Y_{j-})\cos\omega_{mj}t_1 + i(Y_{m+}X_{j-} - Z_{m+}Y_{j-})\sin\omega_{mj}t_1$$

$$\langle I_y^{3,4}\rangle = 2Z_{m+}X_{j-}\sin\omega_{mj}t_1 \qquad \langle I_x^{2,4}\rangle + i\langle I_y^{2,4}\rangle = (Y_{m+}X_{j-} - Z_{m+}Y_{j-})\cos\omega_{mj}t_1 + i(Y_{m+}X_{j-} + Z_{m+}Y_{j-})\sin\omega_{mj}t_1$$

are given in Table 2 where the symbols $I_k^{m,n}$ are fictitious spin-1/2 operators [20]. This 6-by-6 matrix is described only be eighteen independent elements because the density matrix is hermitian. The components associated with the polarizations are located, as expected, along the usual diagonal of the matrix, whereas the other diagonal is occupied by the y-component of the on-resonance coherences. The off-diagonal terms are described by both x- and y-components of single-quantum (1Q) and multi-quantum (MQ) coherences. There is no doubt that, during the pulse, MQ transitions are excited but unfortunately not detectable with a one-pulse experiment. Another property is worth noticing: some line intensities remain unchanged when the $-x$ pulse is changed to an x pulse. This is the case for polarizations, 2Q and 4Q coherences. Only the line intensities of odd-quantum coherences change the sign with that of the pulse.

As previously [19], the matrix multiplications in eqn. (3) are performed using software Mathematica. Actually, only the components of the density matrix related to 1Q coherences, namely, $\rho_{4,3}(t_1, \tau_2, t_3)$, $\rho_{3,2}(t_1, \tau_2, t_3)$, and $\rho_{2,1}(t_1, \tau_2, t_3)$ are required for our propose. The component $\rho_{4,3}(t_1, \tau_2, t_3)$ has the following expression,

$$\begin{aligned}
\rho_{4,3}(t_1, \tau_2, t_3) = \mathrm{i}\{&\langle I_y^{2,5}\rangle C_1 + \langle I_y^{1,6}\rangle C_2 + \langle I_y^{3,4}\rangle C_3 \\
&+ \langle I_z^{2,5}\rangle C_4 + \langle I_z^{1,6}\rangle C_5 + \langle I_z^{3,4}\rangle C_6 \\
&+ \big(\langle I_x^{2,3}\rangle + \langle I_x^{2,4}\rangle\big)(C_7 \sin 2\tau_2\omega_Q + C_8 \cos 2\tau_2\omega_Q) \\
&+ \big(\langle I_x^{2,3}\rangle - \langle I_x^{2,4}\rangle\big)(-C_9 \sin 2\tau_2\omega_Q + C_{10} \cos 2\tau_2\omega_Q) \\
&+ \big(\langle I_x^{1,2}\rangle + \langle I_x^{1,5}\rangle\big)(C_{11} \sin 4\tau_2\omega_Q + C_{12} \cos 4\tau_2\omega_Q) \\
&+ \big(\langle I_x^{1,2}\rangle - \langle I_x^{1,5}\rangle\big)(-C_{13} \sin 4\tau_2\omega_Q + C_{14} \cos 4\tau_2\omega_Q) \\
&+ \big(\langle I_x^{1,3}\rangle + \langle I_x^{1,4}\rangle\big)(C_{15} \sin 6\tau_2\omega_Q + C_{16} \cos 6\tau_2\omega_Q) \\
&+ \big(\langle I_x^{1,3}\rangle - \langle I_x^{1,4}\rangle\big)(-C_{17} \sin 6\tau_2\omega_Q + C_{18} \cos 6\tau_2\omega_Q) \\
&+ \big(\langle I_y^{2,3}\rangle + \langle I_y^{2,4}\rangle\big)(C_7 \cos 2\tau_2\omega_Q - C_8 \sin 2\tau_2\omega_Q) \\
&+ \big(\langle I_y^{2,3}\rangle - \langle I_y^{2,4}\rangle\big)(-C_9 \cos 2\tau_2\omega_Q - C_{10} \sin 2\tau_2\omega_Q) \\
&+ \big(\langle I_y^{1,2}\rangle + \langle I_y^{1,5}\rangle\big)(C_{11} \cos 4\tau_2\omega_Q - C_{12} \sin 4\tau_2\omega_Q) \\
&+ \big(\langle I_y^{1,2}\rangle - \langle I_y^{1,5}\rangle\big)(-C_{13} \cos 4\tau_2\omega_Q - C_{14} \sin 4\tau_2\omega_Q) \\
&+ \big(\langle I_y^{1,3}\rangle + \langle I_y^{1,4}\rangle\big)(C_{15} \cos 6\tau_2\omega_Q - C_{16} \sin 6\tau_2\omega_Q) \\
&+ \big(\langle I_y^{1,3}\rangle - \langle I_y^{1,4}\rangle\big)(-C_{17} \cos 6\tau_2\omega_Q - C_{18} \sin 6\tau_2\omega_Q)\}
\end{aligned} \tag{5}$$

$\rho_{4,3}(t_1, \tau_2, t_3)$ is a pure imaginary quantity. The functions C_i, defined in Table 3, depend on the second pulse length t_3 whereas the line intensities $\langle I_k^{m,n}\rangle$ depend on the first pulse length t_1. The component $\rho_{3,2}(t_1, \tau_2, t_3)$ has the following expression,

$$\begin{aligned}
\rho_{3,2}(t_1, \tau_2, t_3) = &-\langle I_y^{2,5}\rangle(A_1 + \mathrm{i}B_1) - \langle I_y^{1,6}\rangle(A_2 + \mathrm{i}B_2) \\
&-\langle I_y^{3,4}\rangle(A_3 + \mathrm{i}B_3) + \langle I_z^{2,5}\rangle(A_4 + \mathrm{i}B_4) + \langle I_z^{1,6}\rangle(A_5 + \mathrm{i}B_5) \\
&+\langle I_z^{3,4}\rangle(A_6 + \mathrm{i}B_6) + \big(\langle I_x^{2,3}\rangle + \langle I_x^{2,4}\rangle\big)
\end{aligned}$$

$$
\begin{aligned}
&\times\{(A_7+\mathrm{i}B_7)\cos 2\tau_2\omega_Q-(A_8+\mathrm{i}B_8)\sin 2\tau_2\omega_Q\}\\
&+\big(\langle I_x^{2,3}\rangle-\langle I_x^{2,4}\rangle\big)\{(A_9+\mathrm{i}B_9)\cos 2\tau_2\omega_Q+(A_{10}+\mathrm{i}B_{10})\sin 2\tau_2\omega_Q\}\\
&+\big(\langle I_x^{1,2}\rangle+\langle I_x^{1,5}\rangle\big)\{(A_{11}+\mathrm{i}B_{11})\cos 4\tau_2\omega_Q-(A_{12}+\mathrm{i}B_{12})\sin 4\tau_2\omega_Q\}\\
&+\big(\langle I_x^{1,2}\rangle-\langle I_x^{1,5}\rangle\big)\{(A_{13}+\mathrm{i}B_{13})\cos 4\tau_2\omega_Q+(A_{14}+\mathrm{i}B_{14})\sin 4\tau_2\omega_Q\}\\
&+\big(\langle I_x^{1,3}\rangle+\langle I_x^{1,4}\rangle\big)\{(A_{15}+\mathrm{i}B_{15})\cos 6\tau_2\omega_Q-(A_{16}+\mathrm{i}B_{16})\sin 6\tau_2\omega_Q\}\\
&+\big(\langle I_x^{1,3}\rangle-\langle I_x^{1,4}\rangle\big)\{(A_{17}+\mathrm{i}B_{17})\cos 6\tau_2\omega_Q+(A_{18}+\mathrm{i}B_{18})\sin 6\tau_2\omega_Q\}\\
&+\big(\langle I_y^{2,3}\rangle+\langle I_y^{2,4}\rangle\big)\{-(A_7+\mathrm{i}B_7)\sin 2\tau_2\omega_Q-(A_8+\mathrm{i}B_8)\cos 2\tau_2\omega_Q\}\\
&+\big(\langle I_y^{2,3}\rangle-\langle I_y^{2,4}\rangle\big)\{-(A_9+\mathrm{i}B_9)\sin 2\tau_2\omega_Q+(A_{10}+\mathrm{i}B_{10})\cos 2\tau_2\omega_Q\}\\
&+\big(\langle I_y^{1,2}\rangle+\langle I_y^{1,5}\rangle\big)\{-(A_{11}+\mathrm{i}B_{11})\sin 4\tau_2\omega_Q-(A_{12}+\mathrm{i}B_{12})\cos 4\tau_2\omega_Q\}\\
&+\big(\langle I_y^{1,2}\rangle-\langle I_y^{1,5}\rangle\big)\{-(A_{13}+\mathrm{i}B_{13})\sin 4\tau_2\omega_Q+(A_{14}+\mathrm{i}B_{14})\cos 4\tau_2\omega_Q\}\\
&+\big(\langle I_y^{1,3}\rangle+\langle I_y^{1,4}\rangle\big)\{-(A_{15}+\mathrm{i}B_{15})\sin 6\tau_2\omega_Q-(A_{16}+\mathrm{i}B_{16})\cos 6\tau_2\omega_Q\}\\
&+\big(\langle I_y^{1,3}\rangle-\langle I_y^{1,4}\rangle\big)\{-(A_{17}+\mathrm{i}B_{17})\sin 6\tau_2\omega_Q+(A_{18}+\mathrm{i}B_{18})\cos 6\tau_2\omega_Q\} \qquad (6)
\end{aligned}
$$

The functions A_i, defined in Table 4, depend on t_3. The terms B_i are deduced from A_i in substituting N_{mj}, $\sin(\omega_{mj}t_3)$ and $-\cos(\omega_{mj}t_3)$ for L_{mj}, $\cos(\omega_{mj}t_3)$ and $\sin(\omega_{mj}t_3)$, respectively, with

$$N_{mj}=Y_{m+}X_{j-}-Z_{m+}Y_{j-} \qquad (7)$$

The component $\rho_{2,1}(t_1, \tau_2, t_3)$ has the same expression as eqn. (6) except that A_i and B_i have to be replaced with R_i and S_i, respectively. The functions R_i are defined in Table 4. The terms S_i are deduced from R_i in substituting Q_{mj}, $\sin(\omega_{mj}t_3)$ and $-\cos(\omega_{mj}t_3)$ for P_{mj}, $\cos(\omega_{mj}t_3)$ and $\sin(\omega_{mj}t_3)$, respectively, with

$$Q_{mj}=X_{m+}Y_{j-}-Y_{m+}Z_{j-} \qquad (8)$$

Knowledge of these three terms of the density matrix allows the determination of $F_y^{3,4}(t_1, \tau_2, t_3)$, $F_y^{2,3}(t_1, \tau_2, t_3)$, $F_x^{2,3}(t_1, \tau_2, t_3)$, $F_y^{1,2}(t_1, \tau_2, t_3)$ and $F_x^{1,2}(t_1, \tau_2, t_3)$, the *relative* intensity of the central line,

TABLE 3

Functions $C_i(t_3)$ of the density matrix component $\rho_{4,3}(t_1, \tau_2, t_3)$. For clarity, the symbol $\Sigma_{m=1}^{3}\Sigma_{j=1}^{3}$ in front of each term has been omitted

$C_1(t_3)=Y_{m+}Z_{m+}X_{j-}Y_{j-}\cos\omega_{mj}t_3$	$C_4(t_3)=Y_{m+}Z_{m+}X_{j-}Y_{j-}\sin\omega_{mj}t_3$
$C_2(t_3)=X_{m+}Z_{m+}X_{j-}Z_{j-}\cos\omega_{mj}t_3$	$C_5(t_3)=X_{m+}Z_{m+}X_{j-}Z_{j-}\sin\omega_{mj}t_3$
$C_3(t_3)=Z_{m+}Z_{m+}X_{j-}X_{j-}\cos\omega_{mj}t_3$	$C_6(t_3)=Z_{m+}Z_{m+}X_{j-}X_{j-}\sin\omega_{mj}t_3$
$C_7(t_3)=Y_{m+}Z_{m+}X_{j-}X_{j-}\cos\omega_{mj}t_3$	$C_8(t_3)=Y_{m+}Z_{m+}X_{j-}X_{j-}\sin\omega_{mj}t_3$
$C_9(t_3)=Z_{m+}Z_{m+}X_{j-}Y_{j-}\cos\omega_{mj}t_3$	$C_{10}(t_3)=Z_{m+}Z_{m+}X_{j-}Y_{j-}\sin\omega_{mj}t_3$
$C_{11}(t_3)=X_{m+}Z_{m+}X_{j-}Y_{j-}\cos\omega_{mj}t_3$	$C_{12}(t_3)=X_{m+}Z_{m+}X_{j-}Y_{j-}\sin\omega_{mj}t_3$
$C_{13}(t_3)=Y_{m+}Z_{m+}X_{j-}Z_{j-}\cos\omega_{mj}t_3$	$C_{14}(t_3)=Y_{m+}Z_{m+}X_{j-}Z_{j-}\sin\omega_{mj}t_3$
$C_{15}(t_3)=X_{m+}Z_{m+}X_{j-}X_{j-}\cos\omega_{mj}t_3$	$C_{16}(t_3)=X_{m+}Z_{m+}X_{j-}X_{j-}\sin\omega_{mj}t_3$
$C_{17}(t_3)=Z_{m+}Z_{m+}X_{j-}Z_{j-}\cos\omega_{mj}t_3$	$C_{18}(t_3)=Z_{m+}Z_{m+}X_{j-}Z_{j-}\sin\omega_{mj}t_3$

the y- and x-components of an inner satellite, and those of an outer satellite, respectively, defined by:

$$iF_y^{3,4}(t_1, \tau_2, t_3) = \tfrac{2}{35}\,\mathrm{Tr}\left[\rho(t_1, \tau_2, t_3)3iI_y^{3,4}\right] = \tfrac{6}{35}\rho_{4,3}(t_1, \tau_2, t_3) \tag{9a}$$

$$F_x^{2,3}(t_1, \tau_2, t_3) + iF_y^{2,3}(t_1, \tau_2, t_3) = \tfrac{2}{35}\,\mathrm{Tr}\left[\rho(t_1, \tau_2, t_3)\sqrt{8}\left(I_x^{2,3} + iI_y^{2,3}\right)\right] = \frac{2\sqrt{8}}{35}\rho_{3,2}(t_1, \tau_2, t_3) \tag{9b}$$

$$F_x^{1,2}(t_1, \tau_2, t_3) + iF_y^{1,2}(t_1, \tau_2, t_3) = \tfrac{2}{35}\,\mathrm{Tr}\left[\rho(t_1, \tau_2, t_3)\sqrt{5}\left(I_x^{1,2} + iI_y^{1,2}\right)\right] = \frac{2\sqrt{5}}{35}\rho_{2,1}(t_1, \tau_2, t_3) \tag{9c}$$

An important property clearly shown by eqns. (9a)–(9c) is that MQ transitions (symbolized by $\langle I_k^{m,n}\rangle$), not detectable with a one-pulse experiment, are observed indirectly at the end of the second pulse through 1Q coherences. Furthermore, the measurement of the relative line intensity, for a series of the second pulse length t_3, allows the determination of quadrupolar coupling ω_Q [21] for a single crystal, or of quadrupolar coupling constant [22] for a powdered sample.

It is worth noting that these three relative line intensities contain terms that do not depend on the interpulse delay τ_2. They correspond to the first six elements in eqns. (5) and (6). Experimentally, they are verified with an interpulse delay τ_2 as short as possible [23]. For the central transition, the expression is

$$\lambda_y^{3,4}(t_1, t_3) = \tfrac{6}{35}\left(\langle I_y^{2,5}\rangle C_1 + \langle I_y^{1,6}\rangle C_2 + \langle I_y^{3,4}\rangle C_3 + \langle I_z^{2,5}\rangle C_4 + \langle I_z^{1,6}\rangle C_5 + \langle I_z^{3,4}\rangle C_6\right) \tag{10}$$

Fig. 2 shows the graph of $\lambda_y^{3,4}(t_1, t_3)$ *versus* the second pulse length t_3 for three values of $\omega_Q/2\pi$. In the hard pulse excitation case ($\omega_Q \ll \omega_{rf}$), the line intensity of MQ coherences is negligible. Eqn. (10), with

TABLE 4

Functions $A_i(t_3)$ and $R_i(t_3)$ of the density matrix component $\rho_{3,2}(t_1, \tau_2, t_3)$ and $\rho_{2,1}(t_1, \tau_2, t_3)$, respectively. For clarity, the symbol $\frac{1}{2}\Sigma_{m=1}^{3}\Sigma_{j=1}^{3}$ in front of each term has been omitted

$A_1(t_3) = \mathrm{L}_{mj}\mathrm{Y}_{m+}\mathrm{Y}_{j-} \sin \omega_{mj}t_3$	$A_4(t_3) = \mathrm{L}_{mj}\mathrm{Y}_{m+}\mathrm{Y}_{j-} \cos \omega_{mj}t_3$
$A_2(t_3) = \mathrm{L}_{mj}\mathrm{X}_{m+}\mathrm{Z}_{j-} \sin \omega_{mj}t_3$	$A_5(t_3) = \mathrm{L}_{mj}\mathrm{X}_{m+}\mathrm{Z}_{j-} \cos \omega_{mj}t_3$
$A_3(t_3) = \mathrm{L}_{mj}\mathrm{Z}_{m+}\mathrm{X}_{j-} \sin \omega_{mj}t_3$	$A_6(t_3) = \mathrm{L}_{mj}\mathrm{Z}_{m+}\mathrm{X}_{j-} \cos \omega_{mj}t_3$
$A_7(t_3) = \mathrm{L}_{mj}\mathrm{Y}_{m+}\mathrm{X}_{j-} \cos \omega_{mj}t_3$	$A_8(t_3) = \mathrm{L}_{mj}\mathrm{Y}_{m+}\mathrm{X}_{j-} \sin \omega_{mj}t_3$
$A_9(t_3) = \mathrm{L}_{mj}\mathrm{Z}_{m+}\mathrm{Y}_{j-} \cos \omega_{mj}t_3$	$A_{10}(t_3) = \mathrm{L}_{mj}\mathrm{Z}_{m+}\mathrm{Y}_{j-} \sin \omega_{mj}t_3$
$A_{11}(t_3) = \mathrm{L}_{mj}\mathrm{X}_{m+}\mathrm{Y}_{j-} \cos \omega_{mj}t_3$	$A_{12}(t_3) = \mathrm{L}_{mj}\mathrm{X}_{m+}\mathrm{Y}_{j-} \sin \omega_{mj}t_3$
$A_{13}(t_3) = \mathrm{L}_{mj}\mathrm{Y}_{m+}\mathrm{Z}_{j-} \cos \omega_{mj}t_3$	$A_{14}(t_3) = \mathrm{L}_{mj}\mathrm{Y}_{m+}\mathrm{Z}_{j-} \sin \omega_{mj}t_3$
$A_{15}(t_3) = \mathrm{L}_{mj}\mathrm{X}_{m+}\mathrm{X}_{j-} \cos \omega_{mj}t_3$	$A_{16}(t_3) = \mathrm{L}_{mj}\mathrm{X}_{m+}\mathrm{X}_{j-} \sin \omega_{mj}t_3$
$A_{17}(t_3) = \mathrm{L}_{mj}\mathrm{Z}_{m+}\mathrm{Z}_{j-} \cos \omega_{mj}t_3$	$A_{18}(t_3) = \mathrm{L}_{mj}\mathrm{Z}_{m+}\mathrm{Z}_{j-} \sin \omega_{mj}t_3$
with $\mathrm{L}_{mj} = \mathrm{Y}_{m+}\mathrm{X}_{j-} + \mathrm{Z}_{m+}\mathrm{Y}_{j-}$	
$R_1(t_3) = \mathrm{P}_{mj}\mathrm{Y}_{m+}\mathrm{Y}_{j-} \sin \omega_{mj}t_3$	$R_4(t_3) = \mathrm{P}_{mj}\mathrm{Y}_{m+}\mathrm{Y}_{j-} \cos \omega_{mj}t_3$
$R_2(t_3) = \mathrm{P}_{mj}\mathrm{X}_{m+}\mathrm{Z}_{j-} \sin \omega_{mj}t_3$	$R_5(t_3) = \mathrm{P}_{mj}\mathrm{X}_{m+}\mathrm{Z}_{j-} \cos \omega_{mj}t_3$
$R_3(t_3) = \mathrm{P}_{mj}\mathrm{Z}_{m+}\mathrm{X}_{j-} \sin \omega_{mj}t_3$	$R_6(t_3) = \mathrm{P}_{mj}\mathrm{Z}_{m+}\mathrm{X}_{j-} \cos \omega_{mj}t_3$
$R_7(t_3) = \mathrm{P}_{mj}\mathrm{Y}_{m+}\mathrm{X}_{j-} \cos \omega_{mj}t_3$	$R_8(t_3) = \mathrm{P}_{mj}\mathrm{Y}_{m+}\mathrm{X}_{j-} \sin \omega_{mj}t_3$
$R_9(t_3) = \mathrm{P}_{mj}\mathrm{Z}_{m+}\mathrm{Y}_{j-} \cos \omega_{mj}t_3$	$R_{10}(t_3) = \mathrm{P}_{mj}\mathrm{Z}_{m+}\mathrm{Y}_{j-} \sin \omega_{mj}t_3$
$R_{11}(t_3) = \mathrm{P}_{mj}\mathrm{X}_{m+}\mathrm{Y}_{j-} \cos \omega_{mj}t_3$	$R_{12}(t_3) = \mathrm{P}_{mj}\mathrm{X}_{m+}\mathrm{Y}_{j-} \sin \omega_{mj}t_3$
$R_{13}(t_3) = \mathrm{P}_{mj}\mathrm{Y}_{m+}\mathrm{Z}_{j-} \cos \omega_{mj}t_3$	$R_{14}(t_3) = \mathrm{P}_{mj}\mathrm{Y}_{m+}\mathrm{Z}_{j-} \sin \omega_{mj}t_3$
$R_{15}(t_3) = \mathrm{P}_{mj}\mathrm{X}_{m+}\mathrm{X}_{j-} \cos \omega_{mj}t_3$	$R_{16}(t_3) = \mathrm{P}_{mj}\mathrm{X}_{m+}\mathrm{X}_{j-} \sin \omega_{mj}t_3$
$R_{17}(t_3) = \mathrm{P}_{mj}\mathrm{Z}_{m+}\mathrm{Z}_{j-} \cos \omega_{mj}t_3$	$R_{18}(t_3) = \mathrm{P}_{mj}\mathrm{Z}_{m+}\mathrm{Z}_{j-} \sin \omega_{mj}t_3$
with $\mathrm{P}_{mj} = \mathrm{X}_{m+}\mathrm{Y}_{j-} + \mathrm{Y}_{m+}\mathrm{Z}_{j-}$	

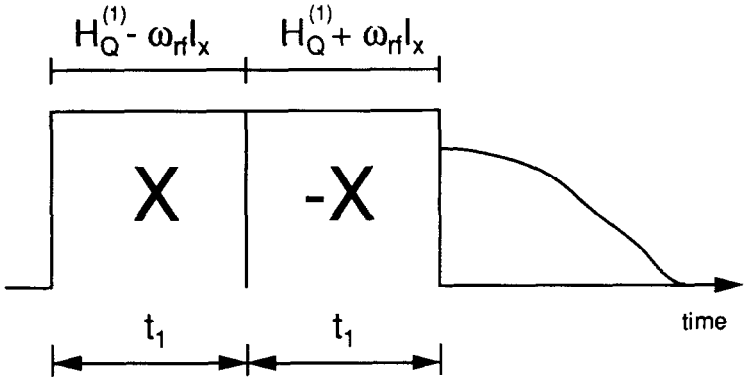

Fig. 3. Rotary echo sequence $\{x\}\{-x\}$–[acquisition(y)]–recycle delay, the two pulse lengths are equal.

the first pulse length corresponding to a $\pi/2$ pulse ($\omega_{rf} t_{90°} = \pi/2$), is equivalent to those given by Weisman and Bennett [16]:

$$\lambda^{3,4}_{y(0)}(t_1 = t_{90°}, t_3) = \tfrac{6}{35}\langle I_y^{3,4}(t_1 = t_{90°})\rangle C_3 \tag{11a}$$

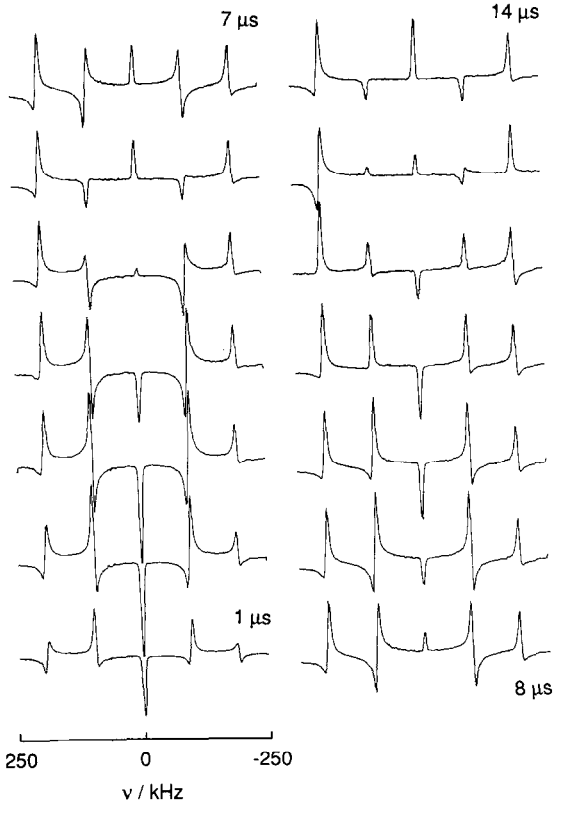

Fig. 4. ^{27}Al spectra of a single crystal of Al_2O_3 acquired with one-pulse excitation.

$$\alpha -\tfrac{9}{2}\Big\{\cos^2\phi\big[\cos^4\phi - 6(\cos\phi\,\sin\phi)^2 + 3\sin^4\phi\big]^2 - \sin^2\phi\big[3\cos^4\phi - 6(\cos\phi\,\sin\phi)^2 + \sin^4\phi\big]^2\Big\} \tag{11b}$$

where $2\phi = \omega_{rf} t_3$ is the second pulse flip angle. In Fig. 2, the curve corresponding to weak ω_Q value is exactly (except the sign because of $-x$ pulses used in the present paper) that of Solomon [15,16] or eqn. (11b).

Even- or odd-quantum detection

The central line intensity [eqn. (5)] depends on a couple of off-resonance coherences, one even- and one odd-quantum. As mentioned above, odd-quantum coherences developed during the first pulse change their sign with that of the pulse. In contrast, even-quantum coherences do not. As a result, alternating the phase of the first pulse without changing that of the receiver (y) will cancel odd-quantum coherences. In other words, the sequence, $\{-x\}$–τ_2–$\{-x\}$–[acquisition(y)]–recycle delay–$\{x\}$–τ_2–$\{-x\}$–[acquisition(y)]–recycle delay, will detect polarization and even-quantum off-resonance coherences. As their line intensities are only important for medium ω_Q values, these line intensities are observed mainly in this condition. The relative intensity of the central line becomes

$$iF_1^{(c)}(t_1, \tau_2, t_3) = \tfrac{6}{35}\rho_{4,3}(t_1, \tau_2, t_3) \tag{12a}$$

with

$$\begin{aligned}\rho_{4,3}(t_1, \tau_2, t_3) = 2i\Big\{&\langle I_z^{2,5}\rangle C_4 + \langle I_z^{1,6}\rangle C_5 + \langle I_z^{3,4}\rangle C_6 \\ &+ \langle I_x^{2,4}\rangle\big[(C_7 + C_9)\sin 2\tau_2\omega_Q + (C_8 - C_{10})\cos 2\tau_2\omega_Q\big] \\ &+ \langle I_x^{1,5}\rangle\big[(C_{11} + C_{13})\sin 4\tau_2\omega_Q + (C_{12} - C_{14})\cos 4\tau_2\omega_Q\big]\end{aligned}$$

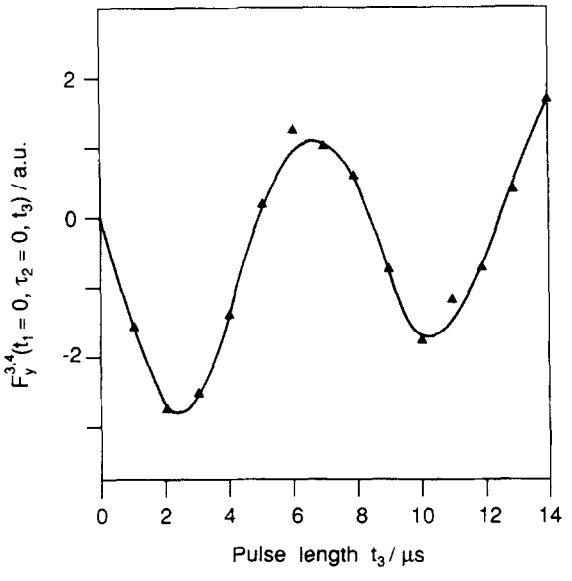

Fig. 5. Fit of ^{27}Al experimental line intensity of Fig. 4 with eqn. (9a), and the parameters: $t_1 = \tau_2 = 0$, $\omega_{rf}/2\pi = 56.4$ kHz and $\omega_Q/2\pi = 47.6$ kHz.

$$+\langle I_x^{1,3}\rangle[(C_{15}-C_{17})\sin 6\tau_2\omega_Q+(C_{16}+C_{18})\cos 6\tau_2\omega_Q]$$

$$+\langle I_y^{2,4}\rangle[(C_7+C_9)\cos 2\tau_2\omega_Q-(C_8-C_{10})\sin 2\tau_2\omega_Q]$$

$$+\langle I_y^{1,5}\rangle[(C_{11}+C_{13})\cos 4\tau_2\omega_Q-(C_{12}-C_{14})\sin 4\tau_2\omega_Q]$$

$$+\langle I_y^{1,3}\rangle[(C_{15}-C_{17})\cos 6\tau_2\omega_Q-(C_{16}+C_{18})\sin 6\tau_2\omega_Q]\} \quad (12b)$$

In contrast, alternating the phase of the first pulse and that of the receiver simultaneously will cancel polarizations and even-quantum off-resonance coherences. In other words, the sequence, $\{-x\}$–τ_2–$\{-x\}$–[acquisition(y)]–recycle delay–$\{x\}$–τ_2–$\{-x\}$–[acquisition($-y$)]–recycle delay, allows the detection of odd-quantum coherences. The relative intensity of the central line becomes

$$iF_2^{(c)}(t_1, \tau_2, t_3) = \tfrac{6}{35}\rho_{4,3}(t_1, \tau_2, t_3) \quad (13a)$$

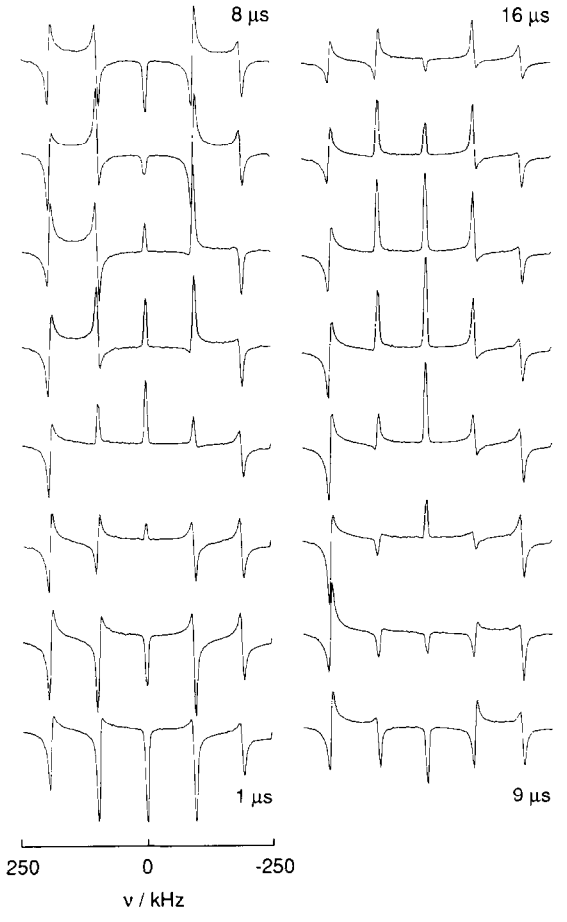

Fig. 6. ^{27}Al spectra of a single crystal of Al_2O_3 acquired with the sequence described in Fig. 1.

with

$$\rho_{4,3}(t_1, \tau_2, t_3) = 2i\{\langle I_y^{2,5}\rangle C_1 + \langle I_y^{1,6}\rangle C_2 + \langle I_y^{3,4}\rangle C_3$$
$$+\langle I_x^{2,3}\rangle[(C_7 - C_9)\sin 2\tau_2\omega_Q + (C_8 + C_{10})\cos 2\tau_2\omega_Q]$$
$$+\langle I_x^{1,2}\rangle[(C_{11} - C_{13})\sin 4\tau_2\omega_Q + (C_{12} + C_{14})\cos 4\tau_2\omega_Q]$$
$$+\langle I_x^{1,4}\rangle[(C_{15} + C_{17})\sin 6\tau_2\omega_Q + (C_{16} - C_{18})\cos 6\tau_2\omega_Q]$$
$$+\langle I_y^{2,3}\rangle[(C_7 - C_9)\cos 2\tau_2\omega_Q - (C_8 + C_{10})\sin 2\tau_2\omega_Q]$$
$$+\langle I_y^{1,2}\rangle[(C_{11} - C_{13})\cos 4\tau_2\omega_Q - (C_{12} + C_{14})\sin 4\tau_2\omega_Q]$$
$$+\langle I_y^{1,4}\rangle[(C_{15} + C_{17})\cos 6\tau_2\omega_Q - (C_{16} - C_{18})\sin 6\tau_2\omega_Q]\} \quad (13b)$$

The expressions of the line intensities in both sequences are simpler than those of the original sequence [eqns. (5) and (9a)]. As a result, the data fitting time will be reduced.

Rotary echo sequence

From now, we deal with the rotary echo sequence ($\{x\}\{-x\}$–[acquisition(y)]–recycle delay) described by two consecutive pulse of opposite phase but of same pulse length (Fig. 3). This sequence represents an alternative way for determining ω_Q. The component $\rho_{4,3}(t_1, t_3 = t_1)$ of the density matrix is simply deduced from eqn. (5). The relative intensity of the central line is

$$iF_3^{(c)}(t_1, t_3 = t_1) = \tfrac{6}{35}\rho_{4,3}(t_1, t_3 = t_1) \quad (14a)$$

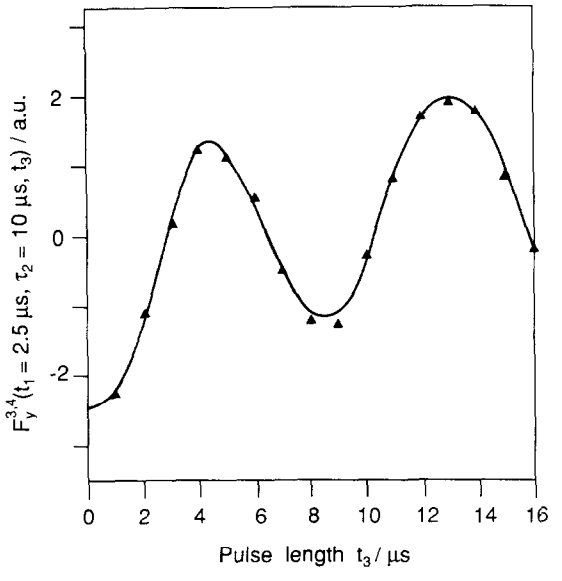

Fig. 7. Fit of ^{27}Al experimental line intensity of Fig. 6 with eqn. (9a), and the parameters: $t_1 = 2.5\ \mu s$, $\tau_2 = 10\ \mu s$, $\omega_{rf}/2\pi = 56.9$ kHz and $\omega_Q/2\pi = 47.5$ kHz.

with

$$\rho_{4,3}(t_1, t_3 = t_1) = \mathrm{i}\Big\{ -\langle I_y^{2,5}\rangle C_1 - \langle I_y^{1,6}\rangle C_2 - \langle I_y^{3,4}\rangle C_3 + \langle I_z^{2,5}\rangle C_4 + \langle I_z^{1,6}\rangle C_5 + \langle I_z^{3,4}\rangle C_6$$
$$- \big(\langle I_x^{2,3}\rangle - \langle I_x^{2,4}\rangle\big) C_8 - \big(\langle I_x^{2,3}\rangle + \langle I_x^{2,4}\rangle\big) C_{10}$$
$$- \big(\langle I_x^{1,2}\rangle - \langle I_x^{1,5}\rangle\big) C_{12} - \big(\langle I_x^{1,2}\rangle + \langle I_x^{1,5}\rangle\big) C_{14}$$
$$+ \big(\langle I_x^{1,3}\rangle - \langle I_x^{1,4}\rangle\big) C_{16} + \big(\langle I_x^{1,3}\rangle + \langle I_x^{1,4}\rangle\big) C_{18}$$
$$- \big(\langle I_y^{2,3}\rangle - \langle I_y^{2,4}\rangle\big) C_7 + \big(\langle I_y^{2,3}\rangle + \langle I_y^{2,4}\rangle\big) C_9$$
$$- \big(\langle I_y^{1,2}\rangle - \langle I_y^{1,5}\rangle\big) C_{11} + \big(\langle I_y^{1,2}\rangle + \langle I_y^{1,5}\rangle\big) C_{13}$$
$$+ \big(\langle I_y^{1,3}\rangle - \langle I_y^{1,4}\rangle\big) C_{15} - \big(\langle I_y^{1,3}\rangle + \langle I_y^{1,4}\rangle\big) C_{17} \Big\} \qquad (14b)$$

Because the first pulse is an x pulse, the signs of odd-quantum line intensities have been changed.

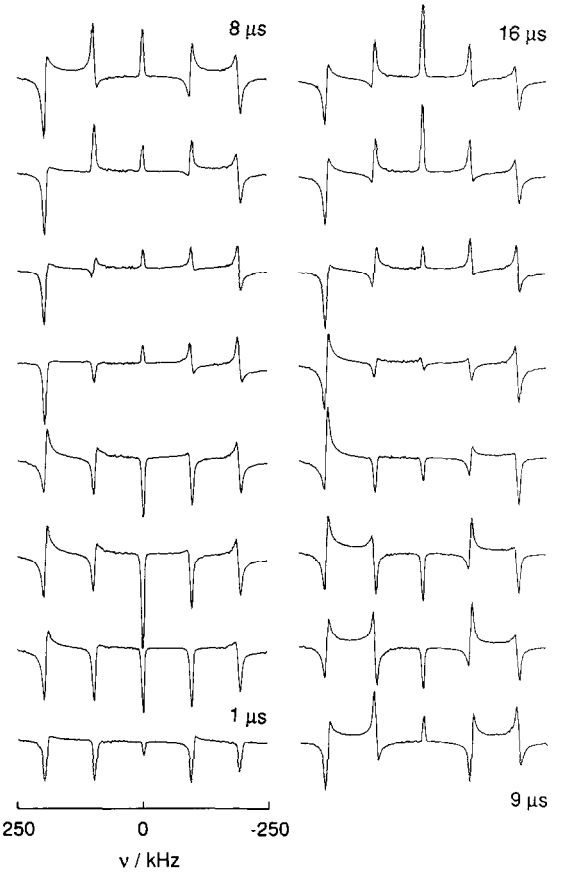

Fig. 8. ^{27}Al spectra of a single crystal of Al_2O_3 acquired with the sequence: $\{-x\}$–τ_2–$\{-x\}$–[acquisition(y)]–recycle delay–$\{x\}$–τ_2–$\{-x\}$–[acquisition(y)]–recycle delay.

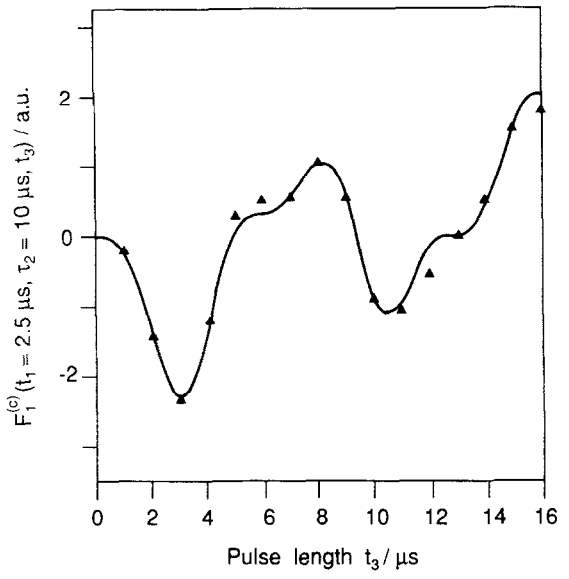

Fig. 9. Fit of ^{27}Al experimental line intensity of Fig. 8 with eqn. (12a), and the parameters: $t_1 = 2.5\ \mu s$, $\tau_2 = 10\ \mu s$, $\omega_{rf}/2\pi = 57.4$ kHz and $\omega_Q/2\pi = 47.2$ kHz.

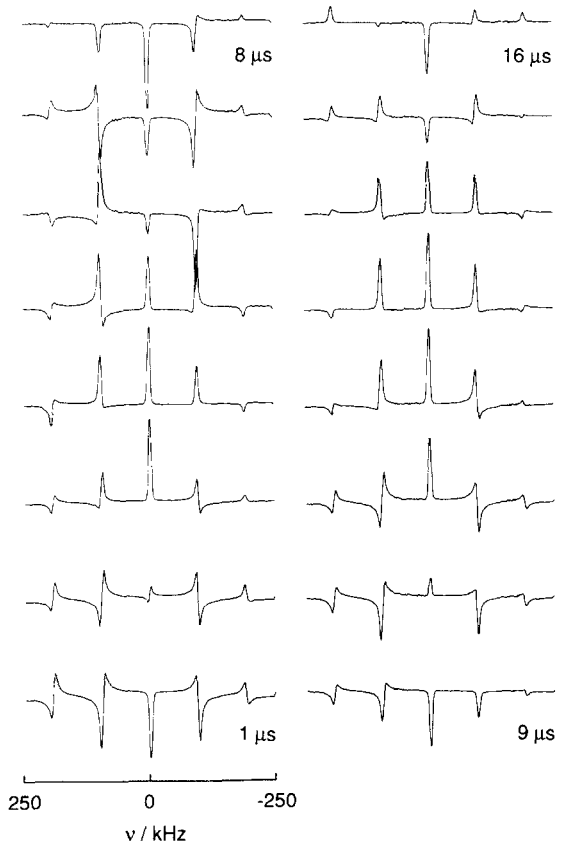

Fig. 10. ^{27}Al spectra of a single crystal of Al_2O_3 acquired with the sequence: $\{-x\}$–τ_2–$\{-x\}$–[acquisition(y)]–recycle delay–$\{x\}$–τ_2–$\{-x\}$–[acquisition($-y$)]–recycle delay.

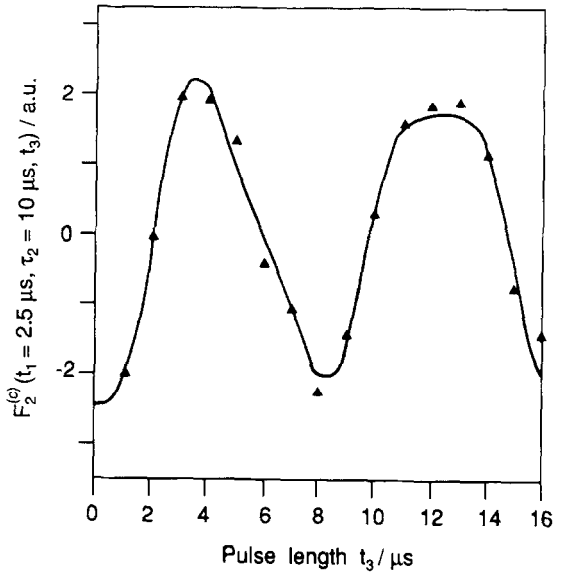

Fig. 11. Fit of ^{27}Al experimental line intensity of Fig. 10 with eqn. (13a), and the parameters: $t_1 = 2.5\ \mu s$, $\tau_2 = 10\ \mu s$, $\omega_{rf}/2\pi = 57.1$ kHz and $\omega_Q/2\pi = 47.6$ kHz.

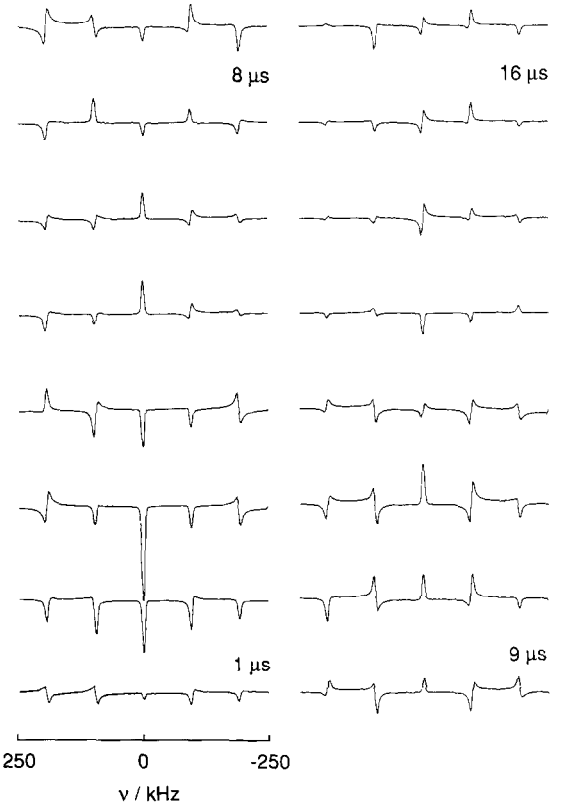

Fig. 12. ^{27}Al spectra of single crystal of Al_2O_3 acquired with the rotary echo sequence (Fig. 3).

Experimental verification

Several analytical expressions of relative line intensity are obtained without taking into account the spin–spin relaxation phenomena as mentioned at the beginning of the previous section. They are required for the study of the Solomon echoes. Otherwise, these relative line intensities can be obtained using numerical methods. In this section, we check their validity with ^{27}Al NMR signals of a single crystal of corundum Al_2O_3.

^{27}Al signals were recorded at room temperature with a Bruker MSL 400 multinuclear high power pulsed NMR spectrometer operating at 104.2 MHz. The high power static probehead was equipped with a 5-mm diameter horizontal solenoid coil. $\omega_{rf}/2\pi = 47$ kHz and the associated $\pi/2$ pulse length $t_{90°} = 5.3$ μs were determined using an aqueous solution. For the one-pulse experiment, the pulse length was incremented from 1 to 14 μs by steps of 1 μs. For the two-pulse experiment, the acquisition parameters were: $t_1 = 2.5$ μs, $\tau_2 = 10$ μs, $t_3 = 1$ to 16 μs by steps of 1 μs. For the rotary echo experiment, the pulse length t_1 was incremented from 1 to 16 μs by steps of 1 μs. In all cases, an acquisition delay of 10 μs, a recycle delay of 10 s and a spectral width of 500 kHz were used. The experimental value of the quadrupolar coupling, which is defined by half the frequency separating two consecutive lines in the spectrum of a single crystal, is $\omega_Q/2\pi = 48$ kHz.

Figs. 4, 6, 8, 10 and 12 show a serie of ^{27}Al spectra acquired with one-pulse excitation, the sequence represented in Fig. 1, the sequence $\{-x\}$–τ_2–$\{-x\}$–[acquisition(y)]–recycle delay–$\{x\}$–τ_2–$\{-x\}$–[acquisition(y)]–recycle delay, the sequence $\{-x\}$–τ_2–$\{-x\}$–[acquisition(y)]–recycle delay–$\{x\}$–τ_2–$\{-x\}$–[acquisition($-y$)]–recycle delay, and the rotary echo sequence represented in Fig. 3, respectively. Due to the large spectral width, only the central line in all the spectra was properly phased. Figs. 5, 7, 9, 11 and 13 present the fit, with the procedure Simplex, of experimental line intensity corresponding to Figs. 4, 6, 8, 10 and 12 with eqns. (9a), (9a), (12a), (13a) and (14a), respectively. The values of ($\omega_{rf}/2\pi$, $\omega_Q/2\pi$) determined with these five sequences are (56.4 kHz, 47.6 kHz), (56.9 kHz, 47.5 kHz), (57.4 kHz, 47.2 kHz), (57.1 kHz, 47.6 kHz), and (54.7 kHz, 49.8 kHz), respectively. The amplitude of the

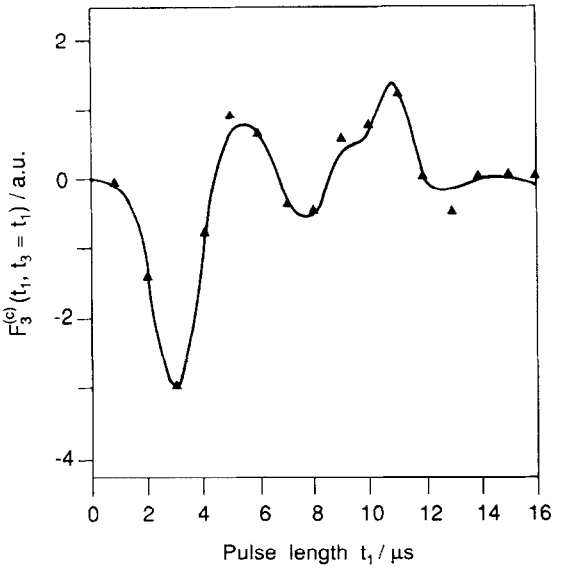

Fig. 13. Fit of ^{27}Al experimental line intensity of Fig. 12 with eqn. (14a), and the parameters: $\omega_{rf}/2\pi = 54.7$ kHz and $\omega_Q/2\pi = 49.8$ kHz.

pulse determined by the fit procedure is about 20% higher than that measured experimentally with an aqueous solution. Otherwise on the whole, the values of ω_Q determined with the fit of the central line intensity *versus* the pulse length are comparable to those provided directly by the spectrum. This represents an alternative way for determining ω_Q when satellite lines are not available. For powdered samples, in cases where the popular MAS method is not applicable, in particular at very low or high temperatures, application of these sequences represents an alternative way for determining the quadrupolar coupling constant and η. As a result, the contribution of the second-order quadrupolar shift (δ_{QS}) to chemical shift can be calculated [2]. The main limitation of these techniques is that they are useful only for a single line. In case of line overlapping, two-dimensional techniques are required to separate lines in the second dimension.

Conclusion

With the help of Mathematica, we have extended the study of spin-5/2 system to two in-phase pulse excitation by including the first-order quadrupolar interaction throughout the experiment. Our results clearly show that (i) single- and multi-quantum coherences developed during the first pulse are detected at the end of the second through single-quantum coherences; and (ii) the line intensity depends not only on the pulse lengths t_1 and t_3 but also on the quadrupolar coupling ω_Q and the amplitude ω_{rf} of the pulse as well. They are valid for any ratio of ω_Q/ω_{rf}. The main restriction is that the interpulse delay τ_2 must be short compared to the duration of fid. Finally, measurement of central line intensity *versus* pulse length allows the determination of quadrupolar parameters.

References

1 D.E. Woessner, *Am. Mineral.*, 74 (1989) 203.
2 E. Lippmaa, A. Samoson and M. Mägi, *J. Am. Chem. Soc.*, 108 (1986) 1730.
3 E. Oldfield, C. Coretsopoulos, S. Yang, L. Reven, H.C. Lee, J. Shore, O.H. Han, E. Ramli and D. Hinks, *Phys. Rev. B*, 40 (1989) 6832.
4 J.C. Edwards and P.D. Ellis, *Langmuir*, 7 (1992) 159.
5 H. Eckert, *Prog. Nucl. Magn. Reson. Spectrosc.*, 24 (1992) 159.
6 N.C. Nielsen, H. Bildsoe and H.J. Jakobsen, *J. Magn. Reson.*, 97 (1992) 149.
7 C. Jäger, W. Müller-Warmuth, C. Mundus and L. van Wüllen, *J. Non-Cryst. Solids*, 149 (1992) 209.
8 J.A.M. Van Der Mijden, R. Janssen and W.S. Veeman, *Mol. Phys.*, 69 (1990) 53.
9 J. Haase and H. Pfeifer, *J. Magn. Reson.*, 86 (1990) 217. J. Haase and E. Oldfield, *J. Magn. Reson.*, 101A (1993) 30.
10 E.W. Wooten, K.T. Mueller and A. Pines, *Acc. Chem. Res.*, 25 (1992) 209.
11 T.H. Walter, G.L. Turner and E. Oldfield, *J. Magn. Reson.*, 76 (1988) 106.
12 P.P. Man, *J. Chim. Phys.*, 89 (1992) 335; *Solid State Nucl. Magn. Reson.*, 1 (1992) 149; *J. Magn. Reson.*, 100 (1992) 157; *Appl. Magn. Reson.*, 4 (1993) 65.
13 B.C. Sanctuary and T.K. Halstead, *Adv. Magn. Opt. Reson.*, 15 (1990) 79.
14 N. Lee, B.C. Sanctuary and T.K. Halstead, *J. Magn. Reson.*, 98 (1992) 534.
15 I. Solomon, *Phys. Rev.*, 110 (1958) 61.
16 I.D. Weisman and L.H. Bennett, *Phys. Rev.*, 181 (1969) 1341.
17 J. Klinowski, *Prog. Nucl. Magn. Reson. Spectrosc.*, 16 (1984) 237.
18 G. Engelhardt and D. Michel, *High-Resolution Solid-State NMR of Silicates and Zeolites*, Wiley, Chichester, 1987.
19 P.P. Man, *Mol. Phys.*, 78 (1993) 307.
20 M. Mehring, E.K. Wolff and M.E. Stoll, *J. Magn. Reson.*, 37 (1980) 475.
21 M.A. Hepp, P.P. Man, A. Trokiner, H. Zanni and J. Fraissard, *Solid-State Commun.*, 84 (1992) 869.
22 P.P. Man, *Chem. Phys. Lett.*, 168 (1990) 227.
23 P.P. Man, *Mol. Phys.*, 72 (1991) 312.